Sensitivity Analysis of Left Atrial Wall Modeling Approaches and Inlet/Outlet Boundary Conditions in Fluid Simulations to Predict Thrombus Formation

Carlos Albors[1(✉)], Jordi Mill[1], Henrik A. Kjeldsberg[2], David Viladés Medel[3], Andy L. Olivares[1], Kristian Valen-Sendstad[2], and Oscar Camara[1]

[1] Sensing in Physiology and Biomedicine (PhySense), Department of Information and Communication Technologies, Universitat Pompeu Fabra, 08018 Barcelona, Spain
carlos.albors@upf.edu

[2] Department of Computational Physiology, Simula Research Laboratory AS, Kristian Augusts Gate 23, 0164 Oslo, Norway

[3] Cardiac Imaging Unit, Cardiology Department, Hospital Santa Creu i Sant Pau, Universitat Autònoma de Barcelona, Sant Antoni Maria Claret 167, 08025 Barcelona, Spain

Abstract. In-silico fluid simulations of the left atria (LA) in atrial fibrillation (AF) patients can help to describe and relate patient-specific morphologies and complex flow haemodynamics with the pathophysiological mechanisms behind thrombus formation. Even in AF patients, LA wall motion plays a non-negligible role in LA function and blood flow patterns. However, obtaining 4D LA wall dynamics from patient-specific data is not an easy task due to current image resolution limitations. Therefore, several approaches have been proposed in the literature to include left atrial wall motion in fluid simulations, being necessary to benchmark them in relation to their estimations on thrombogenic risk. In this work, we present results obtained with computational fluid dynamic simulations of LA geometries from a control and an AF patient with different left atrial wall motion approaches: 1) assuming rigid walls; 2) with a passive movement of the mitral valve annulus plane from a dynamic mesh approach based on springs (DM-SB); and 3) imposing LA wall deformation extracted from dynamic computed tomography (DM-dCT) images. Different strategies for the inlet/outlet boundary conditions were also tested. The DM-dCT approach was the one providing simulation results closer to velocity curves extracted from the reference echocardiographic data, whereas the rigid wall strategy over-estimated the risk of thrombus formation.

Keywords: Computational fluid dynamics · Atrial fibrillation · Left atrial appendage · Dynamic mesh · Thrombus formation · Boundary conditions

O. Camara et al. (Eds.): STACOM 2022, LNCS 13593, pp. 179–189, 2022.
https://doi.org/10.1007/978-3-031-23443-9_17

1 Introduction

Stroke is the main cause of morbidity and mortality from cardiovascular diseases. A primary risk factor is atrial fibrillation (AF), cataloged as the most frequent cardiac arrhythmia in clinical practice and responsible for 15–25% of all ischemic strokes [11]. More than 99% of AF-related strokes originates in an ear-shaped cavity of great morphological variability located in the left atrium (LA), the left atrial appendage (LAA) [3]. Although pharmacological therapies, e.g., oral anti-coagulation (OACS), are first-line therapy for AF patients, left atrial appendage occlusion (LAAO) or excision are also available treatments to prevent and revert the formation process for patients with OAC contra-indications. However, a successful LAAO device implantation requires substantial clinician's experience due to the variability in LAA morphologies and the wide range of device settings to personalise (e.g., design, size, position). Sub-optimal LAAO device choices can lead to abnormal events at follow-up such as device-related thrombosis (DRT), which happens in 2–5% of cases [1,5]. Identifying the LA morphological and haemodynamics characteristics that led to DRT is key to optimise LAAO-based therapy.

Imaging techniques are the gold standard on clinical routine to study LA haemodynamics, specifically Doppler echocardiography images. However, the limited spatial resolution available in these images, representing the flow in one plane and at one time, is not enough to characterise the 4D nature of blood flow patterns in the LA. 4D flow magnetic resonance imaging (4D flow MRI) allows better blood flow characterization, but as a novel modality, it still provides limited LA information [12]. As a potential alternative, in-silico computational fluid simulations (CFD) can help to describe and relate patient-specific LA/LAA morphology and complex hemodynamics to understand the mechanism behind thrombus formation.

Even with the increase in the LA/LAA fluid modeling studies in the literature (see [15] for a recent review), no consensus on optimal boundary conditions have been reached, both for inlet/outlet configurations (i.e., based on pressure and velocities) and LA wall behaviour. The latter is particularly controversial since some researchers [2,8] have assumed rigid LA walls, arguing that LA movement is very limited in AF patients. However, even in those patients, passive movement of the LA induced by the left ventricle (LV) still occurs. Therefore, dynamic mesh approaches using generic mitral valve ring plane excursions [15] or overall LA sinusoidal motion [13] have also been proposed. More advanced strategies have also been used including the extraction of patient-specific LA wall motion from dynamic computed tomography (dCT) images [9,10,17] and fluid-structure interaction (FSI) modelling [4]. Unfortunately, obtaining dCT images of LAAO patients is rarely available in clinical; in parallel, FSI is usually associated to high computational costs and it is uncertain how to define LA wall material properties.

Accordingly, we present in this work a sensitivity analysis on how to incorporate LA wall behaviour in fluid simulations of the left atria and determine the optimal strategy to accurately predict the risk of thrombus formation after LAAO device implantation. The tested strategies were the following: 1) rigid

wall assumption; 2) dynamic mesh with a spring-based method (DM-DB); and 3) dynamic mesh guided by patient-specific dCT data (DM-dCT). Experiments were achieved using dCT imaging from a control and an AF patient, from which echocardiographic data was also available. Several inlet/outlet BC configurations were also studied.

2 Material and Methods

2.1 Clinical Data and 3D Model Generation

Two retrospective cardiac-gated computed tomography angiography images, one from a healthy individual and an AF patient, were provided by Hospital de la Santa Creu i Sant Pau (Barcelona, Spain), after approval by the institutional Ethics Committee and informed consent from patients. The images were acquired with a Somatom Force (Siemens Healthineers, Erlangen, Germany) using a biphasic contrast injection protocol defining a slice thickness of 2 mm without overlapping. In the control case, the full cardiac phase reconstruction was every 1% of the cardiac cycle except for the 34%–48% interval, which was not acquired. For the AF patient, images were acquired at every 5% of the cardiac cycle (0 to 99% of R-R interval). Both LA were segmented from dCT images using semi-automatic tools available in Slicer 4.10.11[1]. 3D surface meshes were created from binary marks out of the segmentation with the flying edges algorithm available in Slicer. Then, volumetric LA geometries were generated from the 3D surface ones using the Gmsh 4.5.4 software[2], with a total of 12×10^5 elements.

2.2 Computational Fluid Dynamic Simulations

Modelling Strategies for Left Atrial Wall Motion. The different approaches to incorporate LA wall motion in fluid simulations for the AF patients were the following: 1) rigid walls; 2) a dynamic mesh method with a spring-based approach (DM-SB) to apply a passive mitral valve (MV) annulus plane movement from literature [18]; and 3) a patient-specific dynamic mesh extracted from the patient's dCT scan (DM-dCT). In the healthy case, only rigid walls and DM-dCT strategies were tested since the second scenario, with only a passive MV movement does not have physiological sense in a non-disease heart.

To extract LA wall motion from the dCT data the first step was to perform the registration of the images acquired every 5% in the AF and 1% in the control case of the cardiac cycle. The image registration step was performed using a concatenation of different models using the ANTs software[3]: (1) rigid registration (i.e., only rotation and translation); (2) affine registration (i.e., adding scaling and shearing); and (3) a symmetric normalization registration (i.e., adding a free-form deformation-based deformable transformation with mutual information as

[1] https://www.slicer.org/.
[2] https://gmsh.info/.
[3] http://stnava.github.io/ANTs/.

optimization metric). The reference mesh always was the cardiac frame starting from ventricular systole (frame 0, i.e., 0% of cardiac cycle). Therefore, 19 and 87 image registrations were performed for the AF and control case, respectively; i.e., in AF from frame 0 to 5, from frame 0 to frame 10 and so on, until reaching the last time-frame of the dCT. For each registration, the output was a matrix of displacements for each image voxel. In addition, the image corresponding to the first time-frame was manually segmented, generating a corresponding 3D surface mesh. Subsequently, displacement matrices extracted from the image registration step were applied to the 3D surface mesh using an piece-wise cubic Hermite interpolating polynomial (PCHIP), displacing the nodes to the following time-frame. MATLAB R2018a (Mathworks, Natick, MS, USA) was used for the image processing and mesh warping steps described above.

The resulting 3D surface mesh and set of displacements at each time-step was then mapped to simulation time in an Ansys file format to be applied as a boundary condition for the LA wall movement. In each simulation time step, a local remeshing process of faces and cells was performed with the proprietary Ansys algorithm lasting 4 min in the DM-dCT approach and 10 min in DM-SB, checking for negative cell volumes and the improvement of the skewness value for mesh quality. Since the nodes were given in DM-dCT, no resolution change has been experienced in the remeshing process. However, changes in mesh resolution of 3–6% were observed in the second modelling strategy.

Boundary Conditions and Simulation Setup. Two boundary condition settings of the inlets/outlets (pulmonary veins/mitral valve) were tested in each of the analysed LA geometrical models. First, a patient-specific velocity profile at the pulmonary veins (PV) was estimated from the derivative of left atrial and left ventricular volume changes measured from the dCT segmented images. In the first BC scenario (Configuration 1), the mitral valve was modelled as a wall during ventricular systole, representing its closing, and a constant pressure value (7 and 8 mmHg for healthy and AF cases, respectively, following [16]) at ventricular diastole, simulating its opening.

In the second BC configuration (Configuration 2), a generic pressure curve was defined at the PV (in sinus rhythm and with AF for the healthy and diseased cases, respectively). A patient-specific velocity profile was defined at the mitral valve, also derived from dCT-derived volume changes of the LA and LV.

To define the passive motion of the mitral annulus in the DM-SB scheme, a displacement function from literature [18] was imposed in the MV annulus plane, describing the longitudinal excursion of the MV. Then, a spring-based dynamic solution of the CFD solver was employed to ensure motion diffusion through the LA wall geometry.

Blood characteristics were set to 1060 kg/m^3 density and the viscosity to 0.0035 Pa/s. Three cardiac cycles were simulated, with a time-step of 0.01 s and 100 steps per beat, according to the heart rate (HR) of each patient. Flow simulations were performed with the Computational Fluid Dynamics solver available in Ansys Fluent 19 R3 (ANSYS Inc, USA), with the following computational resources: Intel i9-9900K CPU, RTX 2080 Ti GPU with 64 Gb RAM. Post-processing and visualization of simulation results were conducted with ParaView

5.8[4]. Computational times ranged between 40–48 h depending on the wall scheme and BC configuration selected.

2.3 In-silico Haemodynamic Indices

The simulated blood flow patterns were qualitatively assessed together with average flow velocities in key LA regions (PV, MV, ostium). Pressure distribution in the LA was also analysed. Moreover, the endothelial cell activation potential (ECAP) was estimated since it has demonstrated to identify regions with high risk of thrombus formation [14]. The mentioned indices were calculated on the third simulated cardiac beat to avoid convergence problems. Additionally, simulated velocity profiles were compared with the estimated from dCT processing in those LA regions where velocity has not been imposed as BC, using the root mean square error (RMSE).

3 Results

The LA displacement fields extracted from dCT images were consistent with patient's conditions, with a MV annular longitudinal excursion of 3 and 9 mm for the AF and healthy case, respectively. Resulting volume change curves from dCT images displayed a volume increase at the maximum diastolic frame of 39 (t = 0.35 s) and 11 (t = 0.45 s) mL for the healthy and AF case, respectively; with slight differences of 4 mL and 3 mL in the same diastolic time frame compared to the volume curves extracted from segmentation in both cases (43 mL and 14 mL for the healthy and AF cases, respectively).

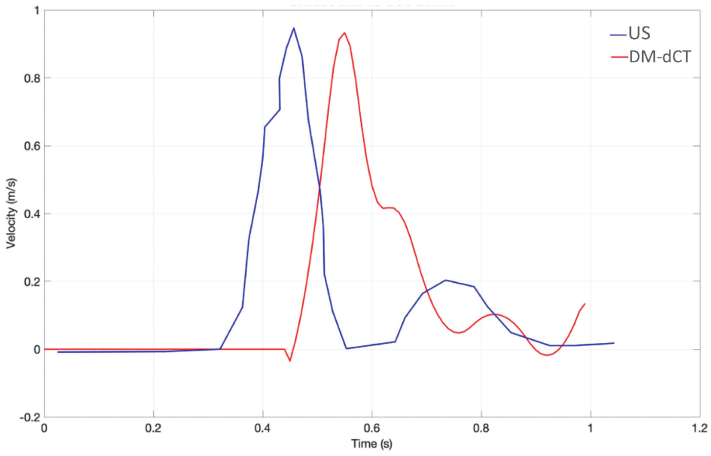

Fig. 1. Velocity curves at the mitral valve (MV) in the AF patient from ultrasound (US) images (blue), and estimated from the left atrial movement derived from dynamic computed tomography (DM-dCT) data (red). (Color figure online)

[4] https://www.paraview.org/.

Figure 1 shows the similarity between the velocity curve in the MV extracted from the dCT and the US data in the AF patient. The velocity magnitudes were in the same range (maximum of 0.94 m/s and 0.93 m/s for US and dCT, respectively). A very small "A-wave" was detected on the US image, even smaller on dCT, with some flow regurgitation (red line in Fig. 1), being a consistent AF behavior. Averaging the results in the two analysed cases, the DM-dCT approach to incorporate LA wall motion into fluid simulations was the one providing velocity curves closer to the ones derived from dynamic imaging (see Fig. 3): RMSE = 0.09 for DM-dCT; RMSE > 0.12 for the remaining strategies (e.g., RMSE of 0.05 and 0.14 for DM-dCT and rigid walls in the control case, respectively). Qualitatively, only the DM-dCT approach faithfully represented the A wave in the control case, as well as correct S waves in the velocity curves at the PV (i.e., a large S1 and a tiny S waves at the healthy and AF cases, respectively, in Fig. 3).

Figure 2 (first two rows) shows how fluid simulations in the control case presented higher velocities and better washout in the LAA than the AF case, as expected. Larger variations in LAA velocities provided by the different BC and LA wall strategies were obtained at the deeper part of the LAA, while they were quite similar at the ostium. The DM-dCT was the approach providing higher blood flow peak velocities (>0.15 m/s even in distal LAA lobes in the healthy case), while the DM-SB and rigid wall strategies gave similar results since the passive MV excursion in the DM-SB did not result in strong motion of the LAA.

As for inlet/outlet BC configurations, defining velocity at the PV (Configuration 1) provided a better blood washout and higher velocities in the LAA and ostium than Configuration 2 BC set-up in the AF patient, while it was the opposite for the control case (see Table 1). Velocity values simulated with the different LA wall motion strategies were quite similar, without a clear distinctive pattern, being less relevant that the inlet/outlet configuration.

Table 1. Average ostium velocities (m/s) during the whole cardiac cycle in a control and an AF patient with the different evaluated boundary conditions and left atrial wall motion approaches. C1 (configuration 1): velocity profile at the inlet pulmonary veins (PV) and pressure constant values at the outlet mitral valve (MV). C2 (configuration 2): pressure at the inlet PV and velocities at the MV outlet. DM-dCT and DM-SB: dynamic mesh approaches guided by dynamic computed tomography images and spring-based method, respectively.

	Control		Atrial fibrillation		
	Rigid	DM-dCT	Rigid	DM-SB	DM-dCT
C1	0.128	0.1495	0.078	0.082	0.08
C2	0.159	0.164	0.084	0.074	0.078

Blood flow patterns were also qualitatively analysed to identify if fluid simulations could reproduce the two main vortices in the LA at end-systolic and

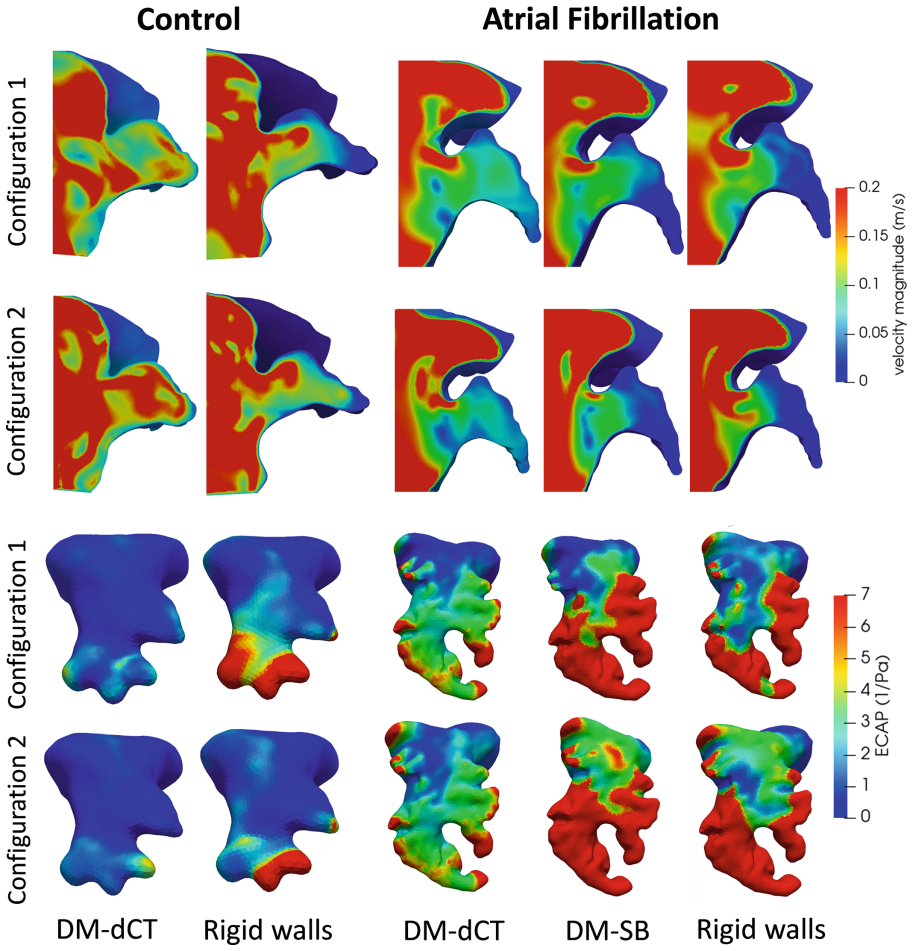

Fig. 2. First two rows: Blood velocity patterns in the left atria (LA) during early diastole (t = 0.6 s) in a control and an AF patient with the different evaluated boundary conditions and left atrial wall motion approaches. Last two rows: Endothelial cell activation (ECAP) maps in a control and an AF patient with the different evaluated boundary conditions and left atrial wall motion approaches. BC configuration 1: velocity profile at the inlet pulmonary veins (PV) and pressure constant values at the outlet mitral valve (MV). BC configuration 2: pressure at the inlet PV and velocities at the MV outlet. DM-dCT and DM-SB: dynamic mesh approaches guided by dynamic computed tomography images and spring-based method, respectively.

mid-diastolic (ventricular) phases reported in 4D flow MRI studies [7]. The DM-dCT approach succeeded to capture both vortices in the control case, with the remaining strategies only reproduced the end-diastolic one (only this one could be seen for all approaches in the AF case). Furthermore, abnormal PV regurgitation was mainly observed in fluid simulations with the DM-SB and rigid wall

strategies to fulfill mass conservation law during ventricular systole, especially with Configuration 1 BC.

The DM-dCT strategy provided the largest PV-MV gradients due to its associated larger LA volume increase compared to the other approaches, which is better observed during ventricular systole. Comparing the evaluated inlet/outlet BC configurations, Configuration 2 generated higher PV-MV pressure gradients than Configuration 1 in both healthy and AF cases (100 Pa and 80 Pa during systole, respectively, for the AF case; 500 Pa and 200 Pa, respectively in the healthy subject), also defining a progressive increase of the LA wall pressure gradient between PV-MV and a MV pressure curve without abrupt changes during valve opening. The reason for instabilities and unrealistic patterns with Configuration 1 BC is the large jump in absolute value pressures when the MV opens (8 mmHg) compared to ventricular systole, when there is not a pressure reference. However, all analysed BC scenarios achieved PV-MV pressure gradients around 70 Pa (i.e., 0.5 mmHg), except during MV opening, which agrees with clinical data. Regionally, higher pressures were found in the LAA at late systole for all analysed BCs, which is consistent with hypothesis on the role of the LAA as a decompression chamber of the LA.

Finally, the ECAP maps displayed in Fig. 2 (last two rows) shows that the DM-dCT achieved the lowest values of ECAP (i.e., lowest risk of thrombus formation) due to the higher blood flow velocity values. As for the DM-SB and rigid schemes, the ECAP distribution maps are similar. Regarding the inlet/outlet BC, differences could not be appreciated in the estimated in-silico thrombogenic indices, being more relevant how to incorporate the LA wall motion strategy into the fluid simulations.

4 Discussion and Conclusions

Computational fluid simulations can provide useful insight to understand the patho-physiological factors behind thrombus formation. However, credibility is a cornerstone of in-silico models requiring personalization, verification and validation with data from different sources (e.g. in-vivo, ex-vivo, etc.), following standards such as the V&V40 guidelines [19]. Comparing different modelling options are then key to establish best practices.

In fluid simulations of the LA, the most important consideration is having a good synchronisation between the LA wall movement, anatomy, and volume changes, with the inlet/outlet parameters (i.e., velocities and pressures) selected at the pulmonary veins and mitral valve, respectively. Left atrial wall motion plays a non-negligible role in simulation scenarios, even in AF patients, although the assumption of rigid walls has been used for years to study them.

Our experiments have demonstrated that incorporating LA wall motion from patient-specific dCT images into fluid simulations is a better strategy than DM-SB and rigid ones, in agreement with recent literature [9]. The DM-dCT was the only LA wall motion strategy able to represent a small S-wave in the PV velocity curves in both patients, which is normally neglected in CFD simulations but

widely reported in clinical studies due to its relationship with several pathologies. In addition, the (largest) LA volume increase defined by the DM-dCT motion at the ventricular systolic phase (MV closure) facilitated the fulfilment of mass conservation law with Configuration 1 BC (i.e., velocities imposed at inlet PV). On the other hand, DM-SB and rigid wall strategies generated non-physiological PV regurgitation to compensate mass imbalance, especially the latter.

One of the main advantages of dCT data is that velocity curves can also be extracted (through mass conservation law) and used them as patient-specific BCs. In our experiments, the resulting dCT velocity curve at the MV was similar to the one measured with ultrasound data (Fig. 1), with equivalent maximum values and with a reduced A wave due to AF. The observed differences in Fig. 1 could be explained by varying patient heartbeat, time between acquisitions, or different positions of velocity measurement in the two modalities. As for the simulated PV velocity curve, it was similar to the one directly derived from dCT data. However, none of them succeeded on properly replicating the complex ventricular systole dynamics at the PV, as already noticed in previous works [10].

Although there were not many global differences in simulated blood flow patterns with the DM-dCT approach (e.g., similar blood flow velocity magnitudes at the ostium), we saw that it led to a better LAA washing and more blood recirculations. Nevertheless, none of the AF tested BC configurations was able to replicate the systolic vortex reported in the literature [6], which could be related to velocity curve inaccuracies.

Combined with the dynamic mesh approach for LA wall motion modelling, Configuration 2 of BC (i.e., imposing velocity at the MV), provided higher ostium velocities in the control case and slightly slower in AF, but more coherent and smooth pressure map distribution in both patients over the cardiac cycle. The DM-SB and rigid wall approaches generated some unrealistic pressure peaks, the latter not creating any pressure differential during ventricular systole. Finally, the thrombogenic ECAP index confirmed the over-estimation of thrombus risk when patient-specific wall motion is not considered due to low time wall shear stress values induced by low/non-existent flow velocities.

Despite the advantages of including LA wall motion from patient-specific dCT data, it is not obvious to acquire such images on a regular basis, being complicated to create large cohorts. Moreover, dCT data still does not fully capture ventricular systole dynamics. Alternatives need to be investigated in the future to transport knowledge on LA wall motion from dCT images available on a small dataset of cases onto each LA to be modelled or to recover as much LA wall motion as possible from 2D-3D echocardiographic data.

Acknowledgement. This project has received funding from the European Union's Horizon 2020 research and innovation programme under grant agreement No 101016496 (SimCardioTest).

A Appendix

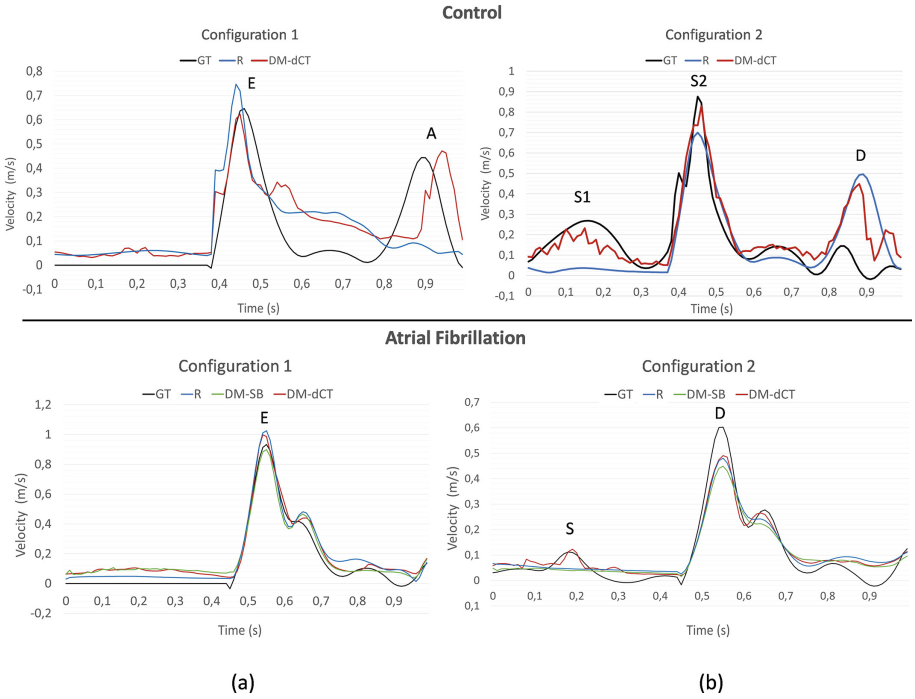

Fig. 3. Validation of the different boundary condition (BC) scenarios in a control and an AF patient. (a) and (b) represents the velocity curves at the mitral valve (MV) and the left superior pulmonary vein (LSPV), respectively, provided by the different approaches for incorporating left atrial wall motion into fluid simulations. Configuration 1: velocity profile at the inlet pulmonary veins (PV) and pressure constant values at the MV outlet. Configuration 2: pressure at the inlet PV and velocities at the MV outlet. GT: Velocity curve extracted from dynamic computed tomography taken as a ground-truth for comparison purposes. R: rigid walls. DM-dCT and DM-SB: dynamic mesh approaches guided by dynamic computed tomography images and spring-based method, respectively.

References

1. Aminian, A., et al.: Incidence, characterization, and clinical impact of device-related thrombus following left atrial appendage occlusion in the prospective global AMPLATZER amulet observational study. JACC: Cardiovasc. Interv. **12**(11), 1003–1014 (2019)
2. Bosi, G.M., et al.: Computational fluid dynamic analysis of the left atrial appendage to predict thrombosis risk. Front. Cardiovasc. Med. **5**, 34 (2018)

3. Cresti, A., et al.: Prevalence of extra-appendage thrombosis in non-valvular atrial fibrillation and atrial flutter in patients undergoing cardioversion: a large transoesophageal echo study. EuroIntervention **15**(3), e225–e230 (2019)
4. Fang, R., Li, Y., Zhang, Y., Chen, Q., Liu, Q., Li, Z.: Impact of left atrial appendage location on risk of thrombus formation in patients with atrial fibrillation. Biomech. Model. Mechanobiology **20**(4), 1431–1443 (2021). https://doi.org/10.1007/s10237-021-01454-4
5. Fauchier, L., et al.: Device-related thrombosis after percutaneous left atrial appendage occlusion for atrial fibrillation. J. Am. Coll. Cardiol. **71**(14), 1528–1536 (2018)
6. Fyrenius, A., Wigström, L., Ebbers, T., Karlsson, M., Engvall, J., Bolger, A.F.: Three dimensional flow in the human left atrium. Heart **86**(4), 448–455 (2001)
7. Garcia, J., et al.: Left atrial vortex size and velocity distributions by 4d flow MRI in patients with paroxysmal atrial fibrillation: Associations with age and CHA2DS2-VASc risk score. J. Magn. Reson. Imaging **51**(3), 871–884 (2020)
8. García-Isla, G., et al.: Sensitivity analysis of geometrical parameters to study haemodynamics and thrombus formation in the left atrial appendage. Int. J. Numer. Methods Biomed. Eng. **34**(8), e3100 (2018)
9. García-Villalba, M., et al.: Demonstration of patient-specific simulations to assess left atrial appendage thrombogenesis risk. Front. Physiol. **12**, 596596 (2021)
10. Gonzalo, A., et al.: Non-newtonian blood rheology impacts left atrial stasis in patient-specific simulations. Int. J. Numer. Methods Biomed. Eng., e3597 (2022)
11. Haeusler, K.G., et al.: Expert opinion paper on atrial fibrillation detection after ischemic stroke. Clin. Res. Cardiol. **107**(10), 871–880 (2018). https://doi.org/10.1007/s00392-018-1256-9
12. Markl, M., et al.: Assessment of left atrial and left atrial appendage flow and stasis in atrial fibrillation. J. Cardiovasc. Magn. Reson. **17**(1), 1–2 (2015)
13. Masci, A., et al.: A proof of concept for computational fluid dynamic analysis of the left atrium in atrial fibrillation on a patient-specific basis. J. Biomech. Eng. **142**(1) (2020)
14. Mill, J., et al.: Patient-specific flow simulation analysis to predict device-related thrombosis in left atrial appendage occluders. REC: Interv. Cardiol. **3**(4), 278–85 (2021)
15. Mill, J., et al.: Sensitivity analysis of in silico fluid simulations to predict thrombus formation after left atrial appendage occlusion. Mathematics **9**(18), 2304 (2021)
16. Nagueh, S.F., et al.: Recommendations for the evaluation of left ventricular diastolic function by echocardiography. Eur. J. Echocardiogr. **10**(2), 165–193 (2009)
17. Otani, T., Al-Issa, A., Pourmorteza, A., McVeigh, E.R., Wada, S., Ashikaga, H.: A computational framework for personalized blood flow analysis in the human left atrium. Ann. Biomed. Eng. **44**(11), 3284–3294 (2016)
18. Veronesi, F., et al.: Quantification of mitral apparatus dynamics in functional and ischemic mitral regurgitation using real-time 3-dimensional echocardiography. J. Am. Soc. Echocardiogr. **21**(4), 347–354 (2008)
19. Viceconti, M., Pappalardo, F., Rodriguez, B., Horner, M., Bischoff, J., Tshinanu, F.M.: In silico trials: verification, validation and uncertainty quantification of predictive models used in the regulatory evaluation of biomedical products. Methods **185**, 120–127 (2021)